Interdisciplinary Research in Medical Sciences Specialty
ISSN: 3062-4401
2025, Volume 5, Issue 1, Page No: 150-165

Available online at: www.galaxypub.co/page/journals

Galaxy Publication

Regulation of Apoptotic and Autophagic Pathways by Propionic Acid in the Ventromedial Hypothalamus of Type 2 Diabetic Rats

Alejandro Fuentes[1], Martín Orozco[1], Sebastián Rivas[1]*

[1]Department of Biomedical Innovation, Faculty of Medicine, University of the Andes, Bogotá, Colombia.

***E-mail** ✉ sebastian.rivas.bio@outlook.com
Received: 28 February 2025; **Revised:** 26 May 2025; **Accepted:** 27 May 2025

ABSTRACT

Hypothalamic dysfunction can lead to irregularities in glucose metabolism, a major contributor to the development of type 2 diabetes mellitus (T2DM). The interplay between autophagy and apoptosis is critical for cellular and tissue balance, and this process may become impaired in T2DM. Given that propionic acid (PA) has neuroprotective properties, this study aimed to explore its impact on the regulation of the apoptosis/autophagy balance in the ventromedial hypothalamus (VMH) of rats with type 2 diabetes mellitus (T2DM). Male Wistar rats were categorized into the following experimental groups: 1) control, 2) T2DM, and 3) treatment groups that received oral doses for 14 days of: 4) metformin (60 mg/kg), 5) sodium salt of propionic acid (PA, 60 mg/kg), and 6) a combination of PA and metformin. Various methods were employed to analyze the effects, including Western blot analysis for proteins such as Bax, Bcl-xl, LC3, Beclin-1, and caspase-3; RT-PCR to quantify gene expression of Bax, Bcl-xl, LC3, and Beclin-1; transmission electron microscopy for ultrastructural assessment; and immunohistochemistry for Bax and Bcl-xl expression in ventromedial hypothalamus (VMH) samples. In rats with T2DM, apoptosis and mitoptosis were observed in the ventromedial hypothalamus (VMH), alongside an enlargement of endoplasmic reticulum (ER) tubules and cisterns. This was accompanied by an imbalance between pro-apoptotic and anti-apoptotic factors, marked by increased levels of Bax and caspase-3, and a reduction in the autophagy marker LC3 and the anti-apoptotic protein Bcl-xl. Treatment with metformin and propionic acid (PA) partially alleviated these ultrastructural changes in the VMH, as evidenced by reduced mitochondrial swelling and fewer apoptotic neurons. Metformin was effective in preventing neuronal apoptosis but also triggered reactive astrogliosis and an accumulation of lipofuscin granules. The increase in the number of autophagosomes was associated with higher levels of LC3, Beclin-1, and Bcl-xl, as well as a decrease in Bax and caspase-3 compared to T2DM alone. PA shifted the cellular response from apoptosis to autophagy by boosting LC3 and Beclin-1 expression, while also elevating Bcl-xl levels. These changes may represent an adaptive mechanism to counteract T2DM-induced apoptosis. Combined treatment with PA and metformin reduced the relative area of ER membranes and cisterns compared to the control, T2DM, and metformin groups. This combined treatment also appeared optimal in restoring the balance between pro-apoptotic, anti-apoptotic, and autophagy markers. Type 2 diabetes mellitus (T2DM) is linked to the activation of apoptosis, which results in functional impairments in the ventromedial hypothalamus (VMH). Physical activity, when combined with metformin, may effectively protect against diabetes-induced neuronal death by shifting the cellular process from apoptosis to autophagy in the VMH.

Keywords: Propionic acid, Metformin, Type 2 diabetes, Ventromedial hypothalamus, Apoptosis, Autophagy

How to Cite This Article: Fuentes A, Orozco M, Rivas S. Regulation of Apoptotic and Autophagic Pathways by Propionic Acid in the Ventromedial Hypothalamus of Type 2 Diabetic Rats. Interdiscip Res Med Sci Spec. 2025;5(1):150-65. https://doi.org/10.51847/xkK5LCRKpf

Introduction

Type 2 diabetes mellitus (T2DM) is the most prevalent chronic metabolic disorder worldwide, a fact emphasized by the World Health Organization (WHO) [1]. A common complication of diabetes is damage to the peripheral and autonomic nervous systems, affecting up to 50% of T2DM patients [2]. Globally, major risk factors contributing to diabetic neuropathy include obesity, lifestyle habits, genetic predispositions, gut microbiota

imbalances, and mitochondrial dysfunction [3]. Diabetes also causes progressive damage to the central nervous system (CNS), including the hypothalamus [4]. Neurons in the ventromedial (VMH), lateral (LHA), and arcuate (ARC) nuclei of the hypothalamus are crucial for maintaining energy balance. T2DM disrupts the molecular pathways and cellular processes in these hypothalamic regions, which may underlie impaired glucose metabolism and be accompanied by neuroinflammation and impaired neurogenesis [5-7]. This suggests a bidirectional relationship between T2DM and hypothalamic dysfunction, with each potentially acting as both a cause and consequence of the other.

Excess glucose and fatty acids have been shown to impair endoplasmic reticulum (ER) function and damage cells [8]. Chronic ER stress can lead to defects in proinsulin synthesis, protein folding, and processing, trigger pro-apoptotic signaling, and initiate mitochondrial apoptosis [9]. The balance between cell survival and death under ER stress is primarily controlled by the unfolded protein response (UPR) signaling. ER stress-induced autophagy is a survival mechanism, likely through the selective removal of disorganized ER and misfolded proteins, a process known as ER-associated degradation (ERAD) [10]. ER stress can regulate autophagy via PERK (protein kinase R-like ER kinase)-mediated pathways [11, 12]. Our previous work demonstrated that elevated PERK levels in the VMH under diabetic conditions are critical for autophagy induction [13]. Therefore, understanding how the switch between apoptosis and autophagy is regulated as a coordinated system for maintaining cellular homeostasis is essential for deciphering T2DM-associated hypothalamic dysfunction.

Autophagy is a fundamental cellular homeostasis process responsible for removing damaged organelles and misfolded proteins via lysosomal degradation under normal conditions [14-16]. In pathological states such as diabetes, autophagy also plays a crucial role [17]. Proper autophagic function is especially important in neurons, which are unable to clear aggregated proteins efficiently [18, 19]. Chronic ER stress, common in neurodegenerative diseases, stimulates autophagy; however, impaired UPR and failure to clear aggregated proteins contribute to neurodegeneration [20, 21]. While the link between ER stress, UPR status, cell death, and neuropathology is partially understood, its role in T2DM-associated hypothalamic dysfunction remains unclear.

Common markers used to study autophagy include Beclin-1 and microtubule-associated protein 1 light chain 3 (LC3). Beclin-1 also plays a role in T2DM progression and has been implicated in diabetic nephropathy [22]. In the brain, Beclin-1-mediated autophagy in the hippocampus may influence cognitive and affective deficits in aged, STZ-induced diabetic mice [23]. LC3 is used to monitor autophagic flux, as its lipidated form (LC3-PE) associates with autophagic membranes [24, 25]. Investigating LC3 and Beclin-1 in T2DM-associated hypothalamic dysfunction is important, as autophagy has been shown to mediate metformin's protective effects against hyperglycemia-induced apoptosis in cardiomyocytes [26].

Apoptosis markers include Bax and Bcl-xl, members of the Bcl-2 family that regulate programmed cell death [27]. Bax promotes apoptosis, whereas Bcl-xl inhibits it, with their ratio reflecting the balance of apoptosis. Neuronal death is believed to contribute to diabetes-induced CNS changes and peripheral neuropathy, yet the dominant mode of cell death—apoptosis or autophagy—in the VMH during T2DM is still unknown.

Pharmacological modulation of UPR signaling and the apoptosis-autophagy interplay may help prevent or treat neurodegeneration. Exploring therapies that target this switch is therefore highly relevant. In this study, we focused on metformin, the most commonly prescribed anti-hyperglycemic drug. As a first-line treatment for T2DM, metformin exhibits anti-hyperglycemic, anti-inflammatory, anti-apoptotic, and antioxidant effects [28, 29]. Its impact on apoptosis and autophagy is context-dependent and varies across cell and animal models. Recent findings indicate that metformin can induce autophagy via AMP-activated protein kinase (AMPK) activation and subsequent inhibition of mammalian target of rapamycin (mTOR), a key autophagy inhibitor, as observed in human gastric adenocarcinoma cells [30].

Combining metformin with a second oral therapy is one approach to improving clinical outcomes. Modern strategies for diabetic neuropathy focus on modulating the gut-brain axis (GBA), particularly mitochondrial function and neuronal energy metabolism. Short-chain fatty acids (SCFAs), including propionate (PA) and acetate, have been shown in animal models to normalize fasting glucose, improve insulin tolerance, and provide metabolic benefits [31]. PA has also been reported to reduce ER stress in bovine mammary epithelial cells [32]. However, conflicting results exist regarding its neurotoxic effects [33]. For example, impaired autophagic flux has been reported in PA-treated hippocampal neurons, accompanied by MAPK/ERK pathway activation [33]. SCFAs also serve as energy sources that protect the intestinal barrier and inhibit autophagy, but their effects on the apoptosis-autophagy balance in T2DM remain unexplored.

Given this background, the present study aimed to investigate the regulatory effects of PA and metformin on the molecular mechanisms governing the apoptosis-autophagy switch in the VMH of rats with experimentally induced T2DM.

Materials and Methods

Animals

Male Wistar rats, aged 2–6 months and weighing 176.8 ± 8.3 g, were used in this study. The animals were maintained under controlled conditions, with a temperature of 24 ± 2 °C, 65 ± 5% humidity, and a 12-hour light/dark cycle. They had unrestricted access to standard rodent chow and water. All experimental protocols adhered to national and international regulations for the ethical treatment of animals, including the European Convention for the Protection of Vertebrate Animals Used for Experimental and Other Scientific Purposes [34] and the Ukrainian Bioethical Guidelines for Preclinical Research (No. 3447-IV, Kyiv, 2006). The study was approved by the Bioethics Committee of Bogomolets National Medical University (Protocol No. 123, dated 23 December 2019).

Experimental design

Each experimental group included 12 rats, which were acclimated for one week prior to the study. The groups were as follows: (1) untreated control; (2) T2DM model induced by a 3-month high-fat diet (HFD) and a single intraperitoneal injection of streptozotocin (STZ, 25 mg/kg body weight, Sigma, USA), followed by 14 days of oral placebo (neutral saline); (3) T2DM rats treated with metformin (GLUKOFAGE, Merck Santé, France) at 60 mg/kg body weight, orally for 14 days; (4) T2DM rats treated with the sodium salt of propionic acid (PROPICUM®, Flexopharm Brain GmbH & Co, Germany) at 60 mg/kg body weight, orally for 14 days; (5) T2DM rats receiving combined treatment with metformin and propionic acid at the same doses and duration. The experimental design is summarized in **Figure 1a**.

T2DM was induced by feeding rats a homogenous HFD containing standard rodent feed (34%), pre-melted lard fat (45%), medical bile acids (1% to enhance fat emulsification and absorption), and dry fructose (20%) [35]. After 3 months of HFD, STZ (25 mg/kg body weight) was administered intraperitoneally [36, 37], followed by a return to standard chow for two weeks [38, 39]. Rats with confirmed T2DM were then randomly allocated to receive oral treatment with placebo, metformin, propionic acid, or their combination for 14 days [40]. The placebo group received an equivalent volume of saline.

At the end of the treatment period, rats were euthanized via decapitation under a lethal dose of sodium thiopental. Blood was collected for serum glucose and glycosylated hemoglobin (HbA1c) measurements. Ventromedial hypothalamus (VMH) samples were carefully dissected for western blot, RT-PCR, and histological analyses. Autophagy markers LC3 and Beclin-1 were evaluated at the transcriptional and protein levels, while apoptosis was assessed by measuring pro-apoptotic markers (Bax, caspase-3) and the anti-apoptotic marker Bcl-xl using RT-PCR, western blot, and immunohistochemistry. Additionally, ultrathin VMH sections were examined by transmission electron microscopy to detect morphological changes and the presence of apoptosis following treatment with metformin, propionic acid, and their combination.

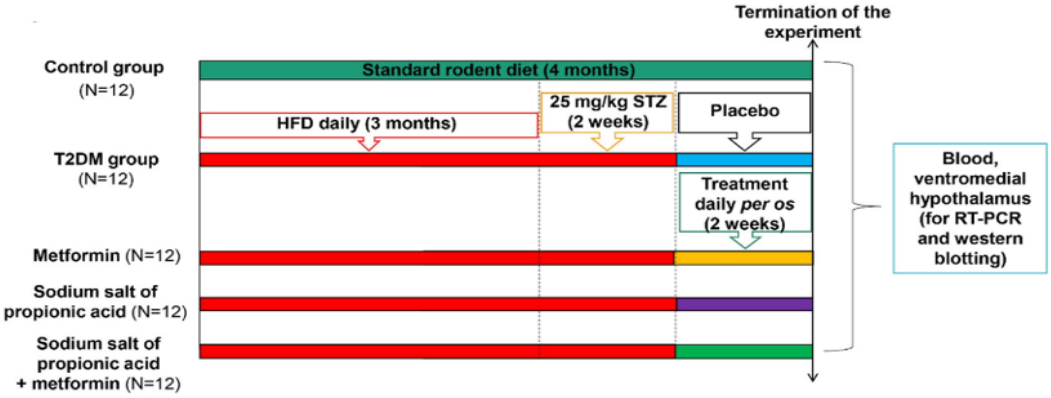

a)

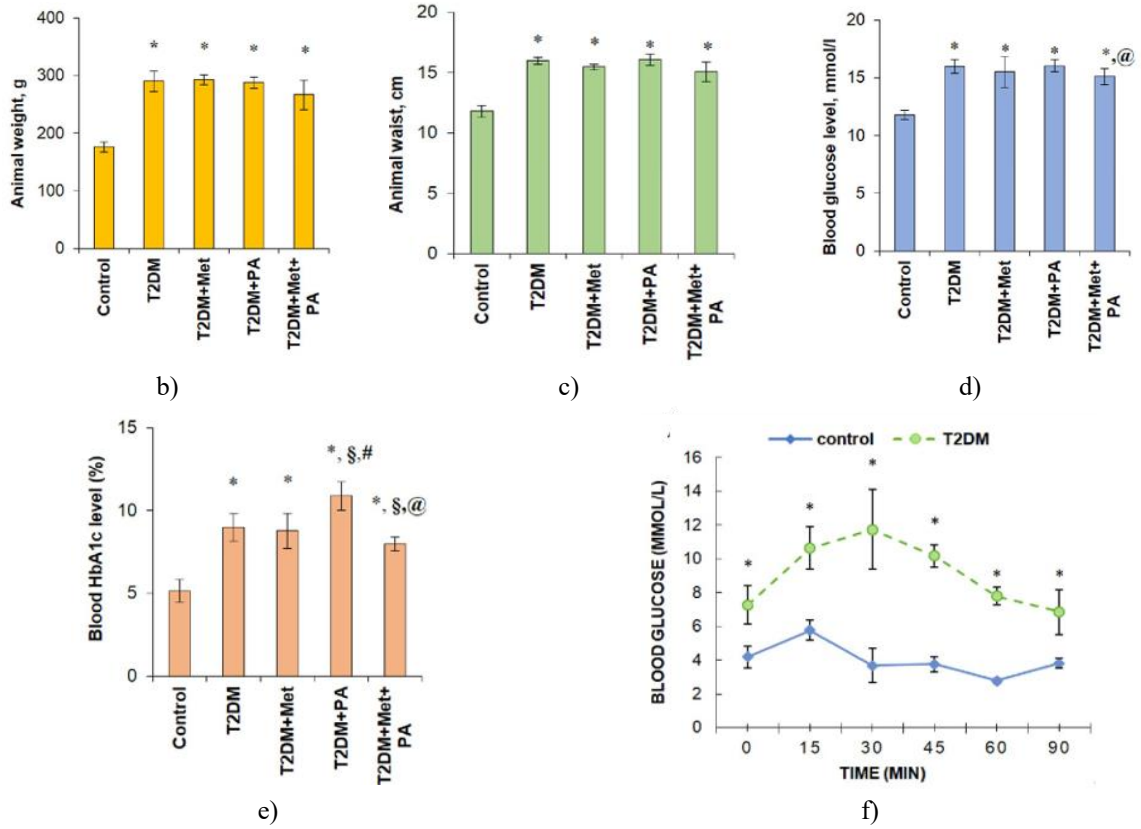

Figure 1. Study design and timeline (a). Type 2 diabetes mellitus was established by feeding rats a high-fat diet for 3 months, followed by a single intraperitoneal injection of streptozotocin (25 mg/kg body weight). Each experimental group contained 12 rats: (1) untreated controls; (2) T2DM model; (3) T2DM treated orally with metformin (60 mg/kg body weight) for 14 days; (4) T2DM treated orally with propionic acid (PA, 60 mg/kg body weight) for 14 days; (5) T2DM receiving combined metformin and PA treatment at the same doses and duration. Panels (b–e) display the effects on body weight (b), waist circumference (c), blood glucose (d), and glycated hemoglobin (HbA1c) levels (e) in diabetic rats and after treatment with metformin or PA. Panel (f) shows the intraperitoneal insulin tolerance test in control rats (n = 6, solid blue line) and T2DM rats (n = 24, dashed green line) prior to treatment. Blood was collected from the tail at specified intervals to measure glucose (mmol/L). Data are shown as mean ± SEM (n = 6); ∗p < 0.05 versus control, §p < 0.05 versus T2DM, #p < 0.05 versus metformin, @p < 0.05 versus PA.

Assessment of glycosylated hemoglobin level

HbA1c levels were quantified using an ion-exchange chromatography and spectrophotometry approach with the HEMOGLOBIN A1C-DIRECT kit (HbA1C-DIR, #31047, Bio Systems, Spain). Fifty microliters of EDTA-anticoagulated whole blood were mixed with 5 mL of distilled water and lysed. The lysate was then applied to the microcolumn provided in the kit, and the elution was carried out with the supplied buffer following the manufacturer's instructions. Absorbance of the eluted HbA1c fraction was measured at 415 nm, alongside total hemoglobin measurements. The proportion of HbA1c was calculated as a percentage of total hemoglobin content.

Slice preparation and electron microscopy

Rat VMH tissue was first fixed in 2.5% glutaraldehyde for 4 hours in Millonig's phosphate buffer (pH 7.4), followed by post-fixation in 1% osmium tetroxide for 1 hour. After brief rinsing in distilled water, the samples were dehydrated through an ascending series of ethanol concentrations (70–100%) and acetone. The tissue was then embedded in a mixture of epon-araldite resin (Epoxy embedding medium #45345-250ML-F, DDSA hardener #45346-250ML-F, Araldite #10951-250ML, Sigma, USA). Semi-thin sections (2–3 µm) were cut to verify the VMH region and stained with methylene blue according to the Hayat method [41]. Ultrathin sections (60–90 nm) were contrasted using 2% uranyl acetate and lead citrate. Observations were performed using a PEM-125

transmission electron microscope (Ukraine) at magnifications ranging from 6,000× to 20,000×. The areas of ER membranes and cisterns within individual cells were measured using ImageJ software.

RNA isolation and quantitative real-time (RT) PCR analysis

For gene expression analysis, total RNA was isolated from 30 mg of ventromedial hypothalamus tissue using the GeneJET RNA Purification Kit (Thermo Fisher Scientific, USA). RNA quality and concentration were evaluated by the OD260/280 and OD260/230 ratios with a DeNovix DS-11 FX+ spectrophotometer (DeNovix Inc., USA). The purified RNA was then reverse-transcribed into cDNA using the RevertAid First Strand cDNA Synthesis Kit (Thermo Fisher Scientific, USA). Quantitative real-time PCR was performed on a 7500 Real-Time PCR System (Life Technologies, USA) with Maxima SYBR Green/ROX qPCR Master Mix (Thermo Fisher Scientific, USA). The thermal cycling protocol included a 10-minute initial denaturation at 95 °C, followed by 40 amplification cycles of 15 seconds at 95 °C and 50 seconds at 60 °C. Primers for the target genes **(Table 1)** were designed using Primer BLAST. Expression levels were normalized to β-actin and calculated as relative fold changes using the ΔΔCt method.

Table 1. The sequences of the primers.

Primer name	Forward primer sequence (5′→3′)	Reverse primer sequence (5′→3′)
Bax	CACGTCTGCGGGGAGTC	CATCCTCTCTGCTCGATCCT
Bcl-xl	GGTCTCTTCAGGGGAAACTG	TCCAAAACACCTGCTCACTC
Beclin-1	GAGGAATGGAGGGGTCTAAGG	TGGCTGTGGTAAGTAATGGAGC
LC3	GTGCATTTGGCTTGGAAACTC	CCTTTTAGAGAAGGCAGCAGG
Gapdh	ACAACAACGAAACCTCCGTG	CACAAGCCCATTTCAGGGTA
β-actin	TGCAGAAGGAGATTACTGCCCTGG	GCTGATCCACATCTGCTGGAAGG

Western blot analysis

The levels of target proteins (LC3, Beclin-1, Bcl-xL, Bax, and caspase-3) were determined using Western blot analysis. Total protein was extracted from frozen hypothalamic tissue samples using RIPA lysis buffer according to a previously described standard protocol [13]. For each sample, 30 μg of protein was loaded per lane and separated by SDS-PAGE on 10–15% polyacrylamide gels (gel percentage selected based on the molecular weight of the target protein). Proteins were subsequently transferred to 0.45 μm nitrocellulose membranes (Merck Millipore, USA; #HATF00010). Membranes were blocked for 1 hour in 5% non-fat dry milk dissolved in PBS containing 0.05% Tween-20 (PBST), then incubated overnight at 4 °C with the following primary antibodies: anti-LC3 (1:1000, Santa Cruz Biotechnology, #sc-134226), anti-Beclin-1 (1:1500, Invitrogen, #PA5-20171), anti-Bcl-xL (1:1000, Invitrogen, #PA5-21676), anti-Bax (1:500, Invitrogen, #MA5-14003), anti-caspase-3 (1:2500, Abcam, #ab208161), and anti-tubulin (1:1000, Sigma-Aldrich, #T5168) as a loading control.

After washing, membranes were incubated with the appropriate HRP-conjugated secondary antibodies: anti-rabbit IgG (1:8000, Sigma-Aldrich, #A0545) or anti-mouse IgG (1:5000, Abcam, #ab97057). Protein bands were visualized by enhanced chemiluminescence using a luminol/p-coumaric acid reagent (Sigma-Aldrich). Band intensities for LC3, Beclin-1, Bcl-xL, Bax, and caspase-3 were quantified relative to tubulin using Gel-Pro Analyzer 32 software (version 3.1).

Immunohistochemical staining and quantification

Immunohistochemistry (IHC) was carried out using polyclonal antibodies against Bax (Invitrogen, USA; #MA5-14003) and Bcl-xL (Invitrogen, USA; #PA5-21676), both diluted 1:500. Staining was visualized with 3,3′-diaminobenzidine (DAB) using the EnVision FLEX detection system (Dako, Denmark).

After the rats were euthanized, transcardial perfusion was performed with 4% paraformaldehyde (PFA) in phosphate-buffered saline (PBS, pH 7.4). Brains were post-fixed overnight in 4% PFA, progressively dehydrated in ascending ethanol concentrations, and embedded in paraplast (Leica-Paraplast Regular, #39601006, Leica Biosystems Inc., USA). Five-micrometer-thick sections of the ventromedial hypothalamus (VMH) were cut on a Microm HM360 microtome (Microm International GmbH, Germany) and mounted on HistoBond®+ adhesive slides (Marienfeld GmbH & Co. KG, Germany). Sections were selected within the stereotaxic range of –2.04 to –3.0 mm caudal to Bregma.

Paraffin was removed by xylene treatment, and sections were rehydrated through a descending ethanol series (100%, 95%, 80%, 70%; 2 min each) followed by two changes of distilled water (2 min each). Heat-induced antigen retrieval was conducted in 10 mM sodium citrate buffer (pH 6.0) at 98 °C for 30 min. Once cooled to 65 °C, slides were rinsed three times (1 min each) in EnVision™ FLEX wash buffer. Endogenous peroxidase was blocked using EnVision FLEX peroxidase-blocking reagent. Sections were incubated with primary antibodies (anti-Bax or anti-Bcl-xL, 1:500) for 30 min, followed by 20 min incubation with HRP-conjugated secondary antibody (EnVision FLEX/HRP). Color was developed for 10 min with a DAB chromogen/substrate mixture (EnVision DAB + Chromogen in EnVision FLEX substrate buffer). Nuclei were counterstained with Gill III hematoxylin.

Sections were examined under an Olympus BX51 microscope, and images were acquired with an Olympus C4040ZOOM digital camera using Olympus DP-Soft version 3.2 software. Staining intensity was scored semi-quantitatively on a 0–4 scale: 0 = no staining or only focal weak staining; 1 = focal strong or diffuse weak staining; 2 = moderate diffuse staining; 3 = strong diffuse staining; 4 = very strong staining.

Statistical analysis

Data normality was assessed with the Shapiro-Wilk test. Inter-group differences were evaluated using one-way analysis of variance (ANOVA) followed by Tukey's post-hoc test. A p-value < 0.05 was regarded as statistically significant. Pearson's correlation coefficient (R) was determined along with its corresponding p-value (at the 95% confidence level). All results were derived from two or three independent experiments and are expressed as mean ± standard error of the mean (SEM). Statistical analyses were conducted using IBM SPSS Statistics software, version 23.0 (SPSS Inc., USA).

Results and Discussion

Influence of metformin and physical activity on body composition, blood glucose regulation, and whole-body insulin sensitivity

The successful induction of type 2 diabetes mellitus (T2DM) following high-fat diet (HFD) was first confirmed by evaluating body parameters (weight and waist circumference), serum glucose and HbA1c levels, and performing an intraperitoneal insulin tolerance test (ipITT).

Compared to control animals, diabetic rats exhibited markedly greater body weight (1.65-fold) and waist circumference (1.35-fold) **(Figures 1b and 1c)**, indicative of obesity. Neither metformin, physical activity (PA), nor their combination significantly reduced body weight or waist circumference relative to the untreated T2DM group, although the combined intervention showed a modest trend toward lower values. All T2DM-related groups still displayed substantially higher body weight (51–67%) and waist circumference than controls, indicating that neither treatment reversed obesity within the study period.

Confirmation of stable hyperglycemia was obtained by measuring fasting blood glucose and HbA1c **(Figures 1d and 1e).** Four weeks after streptozotocin (STZ) injection, fasting glucose in the T2DM group was elevated 1.36-fold compared to controls. Neither metformin nor PA alone significantly lowered glucose levels compared to untreated diabetic rats; however, the combination of metformin + PA produced a modest ~14% reduction relative to PA alone.

HbA1c, a reliable marker of long-term glycemic control, was increased by 74% in the T2DM group and by 70% in the metformin-only group compared to controls. Surprisingly, PA alone further raised HbA1c (2.10-fold vs. control and ~21–24% above T2DM or metformin groups). The metformin + PA combination slightly lowered HbA1c by ~13% versus T2DM alone and by ~37% versus PA alone, yet levels remained 54% above control values.

Overall, persistent hyperglycemia and elevated HbA1c confirmed stable T2DM induction after 3 months of HFD plus a single low-dose STZ injection. Short-term (2-week) treatment with metformin, PA, or their combination produced only minimal improvements in these glycemic parameters.

Whole-body insulin sensitivity was further evaluated by ipITT **(Figure 1f)**. After a 6-hour morning fast, control rats showed the expected transient rise in blood glucose 15 min after insulin injection, followed by a rapid decline, reaching a nadir at 60 min and partial recovery by 75 min. In contrast, T2DM rats started with higher basal glucose (7.26 ± 0.45 mmol/L) and displayed a paradoxical increase (peak 11.73 ± 0.96 mmol/L at 30 min), followed by

slow and incomplete reduction, returning to near-basal levels only after 90 min. These dynamics reflect profound insulin resistance and impaired glucose disposal typical of the T2DM model.

Taken together, the data validate the establishment of obesity, chronic hyperglycemia, elevated HbA1c, and systemic insulin resistance in this HFD + low-dose STZ rat model of T2DM.

Ultrastructural alterations in the ventromedial hypothalamus (VMH) of T2DM rats following metformin and physical activity interventions, as evaluated by transmission electron microscopy

In the second part of the study, we sought to answer two key questions: (1) what ultrastructural alterations occur in VMH neurons in rats with type 2 diabetes, and (2) how do metformin and physical activity (PA), either alone or in combination, affect overall cellular architecture and organelle morphology. To address these aims, transmission electron microscopy (TEM) was employed.

In control animals, VMH neurons displayed normal ultrastructure **(Figures 2a and 2b).** Nuclei were distinct with evenly distributed chromatin and a narrow perinuclear cisterna continuous with the rough endoplasmic reticulum. The Golgi apparatus was prominent and well-organized, and mitochondria exhibited intact cristae and distinct outer membranes. Occasionally, isolated small autophagosomes and lysosomes were observed, consistent with basal autophagic activity in healthy neurons.

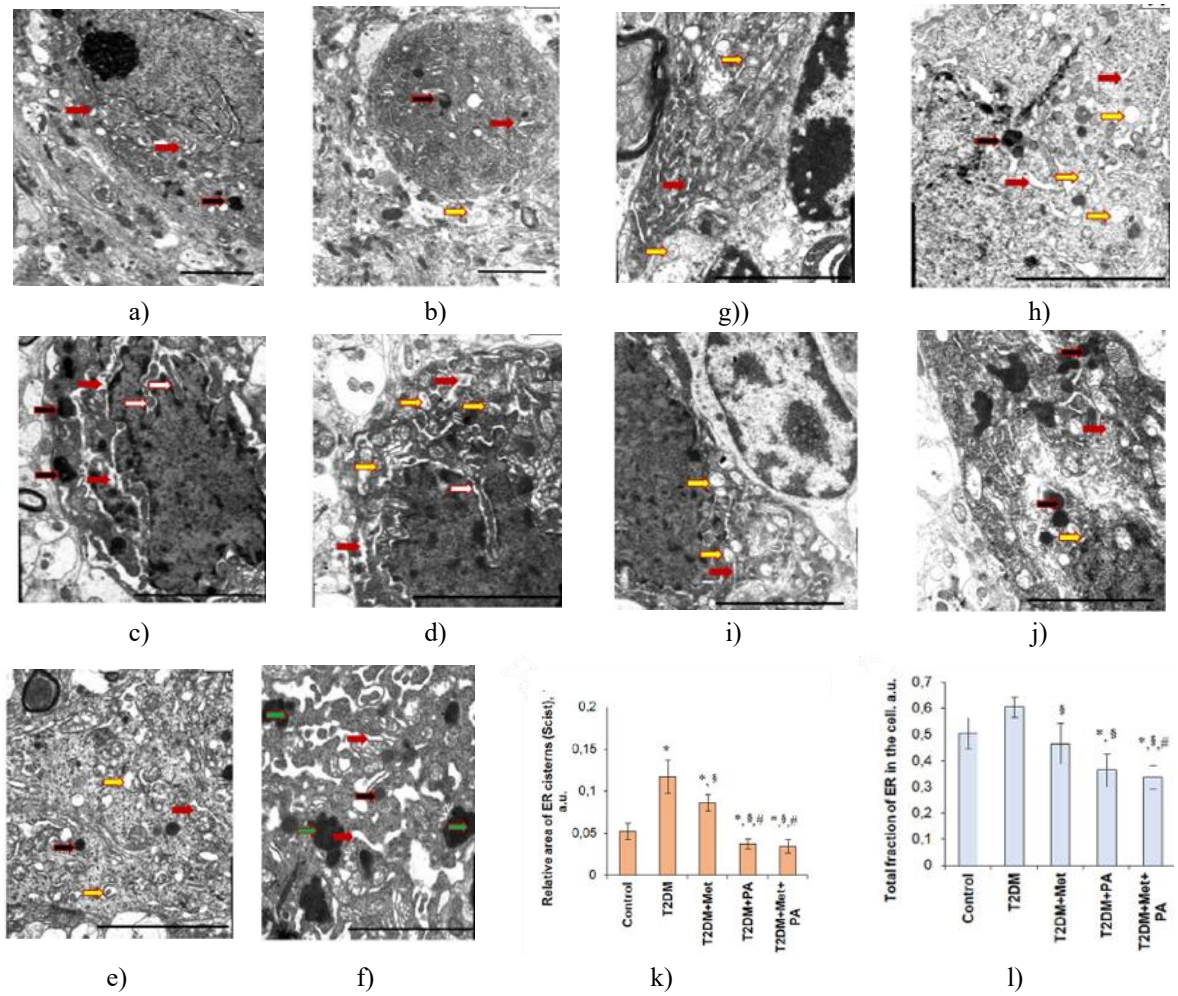

Figure 2. Transmission electron microscopy revealed marked ultrastructural pathology in VMH neurons of T2DM rats **(Figures 2c, 2d)**. Compared to control neurons **(Figures 2a, 2b)**, diabetic neurons exhibited increased electron density of both cytoplasm and nucleoplasm. The Golgi apparatus showed partial fragmentation, rough endoplasmic reticulum (RER) tubules were dilated, and most mitochondria displayed severe damage, including cristolysis, matrix edema, and membrane disruption. Occasional mitophagosomes were noted. Autophagosomes (**Figure 2d**, yellow arrows) and lysosomes (**Figure 2c**, black arrows) appeared more frequently than in controls. Nuclear pyknosis with deep membrane invaginations (**Figures 2c, 2d**, white arrows) was common, and rare nuclear fragmentation was observed. The neuronal population was dominated

by “dark” (pre-apoptotic/apoptotic) neurons with shrunken dendrites and axons; “light” neurons were virtually absent. Synaptic terminals in the neuropil were swollen with vesicle depletion, and perineuronal astrocytes showed cytoplasmic edema and organelle loss.

Metformin monotherapy provided limited protection **(Figures 2e and 2f)**. The Golgi complex regained visibility, RER cisterns appeared closer to normal, and mitochondrial damage was somewhat reduced compared to untreated T2DM. However, lipofuscin granules accumulated prominently **(Figure 2f)**, (green arrows), autophagosomes and lysosomes remained numerous, and reactive astrogliosis with astrocytic hypertrophy was evident. Axonal swelling and myelin damage persisted.

Physical activity (PA) alone yielded more pronounced beneficial effects **(Figures 2g and 2h)**. Intracellular membranes, particularly RER tubules with abundant surface ribosomes, were well preserved and resembled control morphology. Two distinct autophagosome populations were observed: primary (double-membrane) and secondary (single-membrane containing degraded material), possibly reflecting enhanced clearance of misfolded proteins. The proportion of “dark” apoptotic neurons decreased markedly, while “light” neurons with pale nuclei predominated. Nuclear membrane invaginations were more frequent than in controls, and mild perinuclear space widening occurred in some cells—features suggestive of compensatory nucleo-cytoplasmic exchange. Astrocytes showed no edema.

Combined metformin + PA treatment **(Figures 2i and 2j)** further reduced the number of pre-apoptotic and apoptotic neurons compared to either intervention alone and increased microglial presence in the VMH. In “light” neurons, RER tubules were clearly delineated but carried fewer ribosomes **(Figures 2i and 2j)**, (red arrows); in remaining “dark” neurons, ER cisterns and vesicles stayed dilated. Swollen mitochondria, lysosomes **(Figure 2j)** (black arrows), and lipofuscin were still elevated versus controls but lower than in T2DM or metformin-only groups. Nuclear invaginations were particularly pronounced in “light” neurons, and perineuronal astrocytic swelling was less severe than in untreated diabetes.

Overall, T2DM induced extensive organelle fragmentation (especially mitochondria), ER stress, apoptotic neuronal loss, and neuropil edema. Both interventions partially counteracted these changes, with PA showing greater efficacy than metformin in preserving cytoarchitecture, reducing apoptotic neurons, and normalizing glial responses. The combination provided additive benefits in several parameters.

Given the established role of ER stress in obesity-related leptin/insulin resistance, quantitative morphometry of ER was performed using ImageJ on electron micrographs **(Figures 2k and 2l)**;(n = 12 neurons/group). T2DM caused a 2.25-fold increase in ER cisternal area and a non-significant 19% rise in total ER fractional area. All treatments significantly reduced both parameters, often below control levels: metformin lowered cisternal area by 36% (vs. T2DM) but still 65% above control; PA produced the strongest reductions (cisternal area ↓40.5% vs. control, ↓316% vs. T2DM; total ER fraction ↓39% vs. control, ↓66% vs. T2DM); the combination achieved the greatest normalization (cisternal area ↓53% vs. control, ↓344% vs. T2DM; total ER fraction ↓50% vs. control, ↓80% vs. T2DM). Thus, despite initial ER dilation in T2DM, metformin, PA, and especially their combination markedly reduced ER membrane and luminal compartments, in some cases overshooting control values **(Figures 2k and 2l).**

Effects of metformin and physical activity on apoptosis- and autophagy-related protein markers in the ventromedial hypothalamus of rats with type 2 diabetes mellitus

Given the increased autophagosome numbers observed under electron microscopy in treated T2DM rats, we next evaluated autophagic activity by quantifying two key markers: LC3 and Beclin-1. LC3, a well-established mammalian autophagosomal membrane protein, is widely used to monitor autophagy flux in various pathological conditions, including neurodegeneration, neuromuscular disorders, cancer, and infections [42].

In the untreated T2DM group, LC3-II protein levels were reduced by 25% relative to controls **(Figures 3a and 3b)**, indicating mild suppression of autophagy. Treatment markedly reversed this deficit: metformin increased LC3-II by 1.82-fold, physical activity (PA) by 3.95-fold, and the combination by 2.79-fold compared with the T2DM group. In contrast, LC3 mRNA expression showed no significant inter-group differences (**Figure 3c),** demonstrating that the observed changes were primarily post-transcriptional/translational rather than transcriptional.

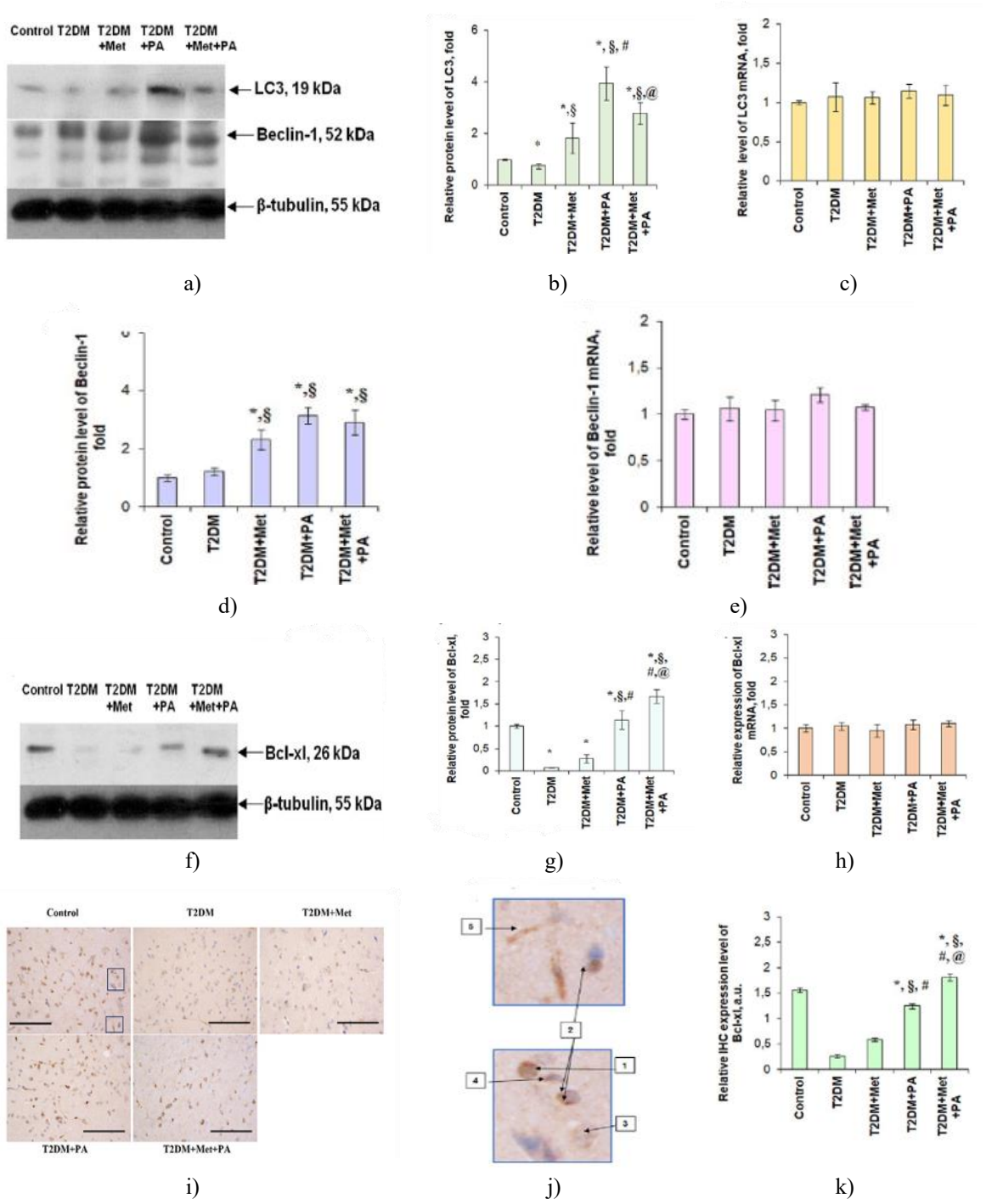

Figure 3. Beclin-1, a critical regulator of autophagy initiation and membrane trafficking that resides mainly in the endoplasmic reticulum, mitochondria, and perinuclear membrane [43].

In contrast to LC3, Beclin-1 protein levels showed no significant difference between control and untreated T2DM groups. However, all treatments markedly elevated Beclin-1: metformin by 2.33-fold, PA by 3.15-fold, and the combination by 2.91-fold compared with the T2DM group **(Figures 3a and 3d)**. As with LC3, Beclin-1 mRNA expression remained unchanged across all groups **(Figure 3e)**, confirming that regulation occurred predominantly at the translational level. These parallel increases in both LC3-II and Beclin-1 strongly indicate that metformin and especially PA (alone or combined) activate autophagy in the VMH of diabetic rats.

Given that Beclin-1 can suppress apoptosis through interaction with the Bcl-2/Bcl-xL complex [44], we next examined the Bax/Bcl-xL apoptotic axis. T2DM dramatically reduced the anti-apoptotic protein Bcl-xL by approximately 90% (10-fold decrease) compared with controls **(Figure 3f and 3g)**. Metformin produced only a modest recovery of Bcl-xL, whereas PA alone and the metformin + PA combination restored (and even exceeded)

control levels, reaching +14% and +67% above control, respectively. Bcl-xL mRNA levels showed no significant changes **(Figure 3h)**, again pointing to post-transcriptional regulation.

Immunohistochemical analysis corroborated the Western blot findings **(Figures 3i–3k)**. In control VMH, Bcl-xL was prominently expressed in neurons (as intensely stained perinuclear macules and occasional diffuse cytoplasmic staining), glial cells (perinuclear granules), and vascular endothelium **(Figure 3k)**. T2DM virtually abolished detectable Bcl-xL in all cell types, with only faint diffuse neuronal staining remaining. Metformin partially restored perinuclear macules in neurons and weak glial/endothelial staining. PA alone nearly normalized expression, producing larger and more intensely stained macules in neurons and stronger glial immunoreactivity. The combination yielded the strongest signal: neuronal macules were larger and more intense than in controls, glial staining was markedly enhanced, and endothelial expression returned to control levels **(Figures 3j and 3i).** Thus, PA and especially metformin + PA robustly reactivated the anti-apoptotic Bcl-xL pathway in neurons, glia, and vasculature of the diabetic VMH.

Finally, we assessed the pro-apoptotic protein Bax. Western blotting revealed a 5.16-fold increase in monomeric Bax in the T2DM group compared with controls (**Figures 4a and 4b)**, consistent with enhanced apoptotic signaling.

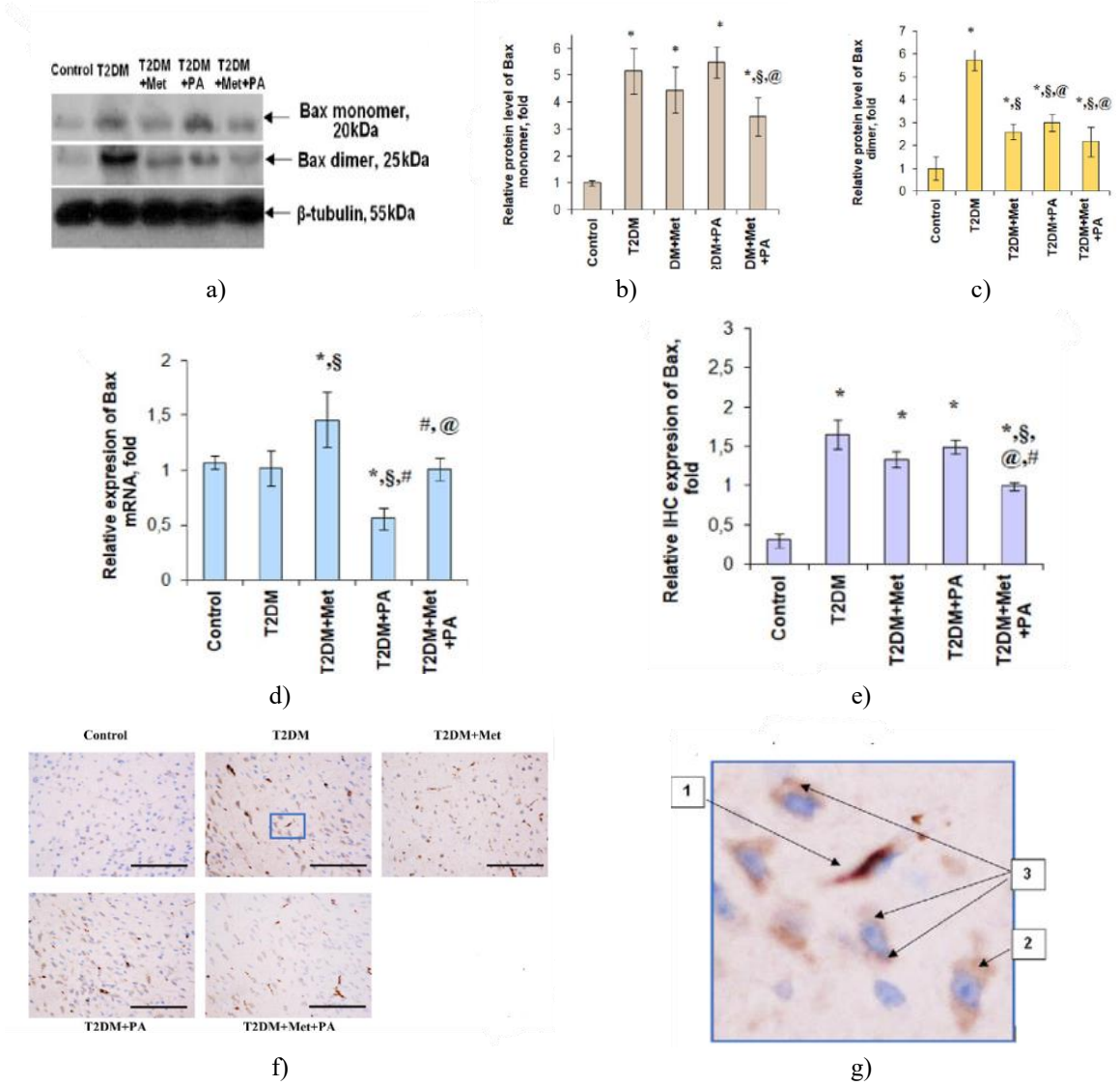

h) i)

Figure 4. Effects of metformin and physical activity on apoptotic and anti-apoptotic markers in the VMH of T2DM rats

Western blot analysis of Bax revealed distinct monomeric (~21 kDa) and dimeric (~42 kDa) bands **(Figures 4a–4c)**. In the T2DM group, monomeric Bax was elevated 5.16-fold versus control. Neither metformin nor PA alone reduced monomeric Bax, but their combination lowered it 1.5-fold compared to untreated T2DM **(Figure 4b).** In contrast, all treatments significantly decreased the Bax dimer: metformin by 2.2-fold, PA by 1.9-fold, and the combination by 2.7-fold relative to T2DM **(Figure 4c)**.

Bax mRNA levels in T2DM were unchanged from control. Metformin alone increased Bax mRNA 1.45-fold above both control and T2DM levels, consistent with its known pro-apoptotic action in certain contexts (e.g., via ERK/p53 signaling in cancer cells [45]). PA alone reduced Bax mRNA 1.81-fold versus T2DM. When combined, the opposing effects canceled out, returning Bax mRNA to near-control/T2DM levels **(Figure 4d)**.

Immunohistochemical semi-quantitative scoring corroborated the protein data **(Figures 4e–4g).** Control VMH showed low-to-moderate Bax staining in endothelium, sparse cytoplasmic/nuclear labeling in neurons, and minimal glial expression. T2DM dramatically upregulated Bax, especially in vascular endothelium **(Figures 4g and 1)**, with strong cytoplasmic neuronal staining (**Figures 4g and 2)** and perinuclear glial granules **(Figure 4g and 3)**. Metformin slightly attenuated this increase, whereas PA alone had little effect. Strikingly, combined metformin + PA markedly reduced Bax immunoreactivity across all cell types, although levels remained ~3-fold above control. Endothelial staining decreased noticeably, neuronal intensity was lower than in single-treatment groups, and glial Bax shifted predominantly to perinuclear localization **(Figures 4e and 4f).**

These findings suggest that T2DM promotes Bax oligomerization (reflected by elevated dimers) and translocation, particularly in the vasculature, potentially contributing to diabetes-related endothelial dysfunction in the VMH. Only the combined intervention effectively suppressed both monomeric and dimeric pro-apoptotic Bax.

Caspase-3, a key executioner caspase, was dramatically elevated 4.4-fold in the VMH of T2DM rats (**Figurea 4h and 4i)**. All treatments reduced cleaved caspase-3: metformin produced the largest drop (8.8-fold vs. T2DM), followed by the combination (2.93-fold) and PA alone (1.94-fold). Despite these reductions, caspase-3 remained ~1.5–6-fold higher than in controls, indicating persistent, albeit attenuated, apoptotic execution.

In summary, T2DM triggered robust pro-apoptotic signaling in the VMH, characterized by massive upregulation of monomeric and dimeric Bax and cleaved caspase-3. Metformin and especially the metformin + PA combination exerted the strongest anti-apoptotic effects, significantly lowering both Bax forms and caspase-3, while markedly restoring the anti-apoptotic protein Bcl-xL .

Pearson's correlation analysis further clarified the interplay between autophagy and apoptosis markers **(Table 2).** Strong positive correlations were observed between the autophagy markers Beclin-1 and LC3 (r high), Beclin-1 and Bcl-xL, and LC3 and Bcl-xL, supporting coordinated activation of autophagy and anti-apoptotic pathways. Conversely, Bax and caspase-3 were strongly positively correlated, whereas caspase-3 exhibited a strong negative correlation with Bcl-xL, fully consistent with their opposing roles in cell fate determination. These relationships reinforce the conclusion that metformin and PA, particularly in combination, shift VMH neurons from apoptosis toward protective autophagy.

Table 2. Pearson's correlation matrix illustrating the relationships among autophagy and apoptosis markers in the ventromedial hypothalamus of rats.

	Beclin-1	**Caspase-3**	**Bcl-xl**	**Bax dimer**	**LC3**
Beclin-1	1	-,042	,537**	,061	,781**
Caspase-3	-,042	1	-,417*	,779**	-,109
Bcl-xl	,537**	-,417*	1	-,344	,477*
Bax dimer	,061	,779**	-,344	1	-,214
LC3	,781**	-,109	,477*	-,214	1

Note: * - p< 0.05; ** - p <0.01.

Because the balance between neuronal survival and loss in the hypothalamus can affect the regulation of feeding [46], this study set out to determine whether a high-fat diet (HFD) can trigger apoptosis and/or autophagy in cells of the ventromedial hypothalamus (VMH), and to explore how potential neuroprotective strategies used together with metformin might modulate these cell-death pathways. Autophagy, a stress-induced catabolic mechanism, can promote cellular adaptation and survival, but under certain conditions can also contribute to cell death [47]. Although autophagy and apoptosis differ mechanistically, several proteins regulate both pathways, acting as molecular "switch points" that may be exploited therapeutically [48]. For example, the anti-apoptotic proteins Bcl-2 and Bcl-xl inhibit both autophagy and apoptosis through their interactions with Beclin-1 and Bax/Bak, respectively, via their BH3-binding pockets [49, 50]. It has been suggested that phosphorylation of Bcl-2/Bcl-xl may serve as a regulatory mechanism determining whether cells undergo apoptosis or autophagy [51]. Because impaired autophagy has been associated with the onset of neurodegenerative disorders [52], the present study focused on the interaction between apoptosis and autophagy in the VMH following treatment with metformin and propionic acid (PA). To do so, we assessed the expression of pro-apoptotic proteins (Bax, caspase-3), anti-apoptotic proteins (Bcl-xl), and autophagy-related proteins (LC3, Beclin-1) in the VMH of rats with T2DM and following intervention.

A central objective of this work was to identify possible therapeutic means to counteract diabetes-related pathology in the VMH. We therefore examined how metformin and sodium propionate influence apoptosis and autophagy in the hypothalamus as potential neuroprotective approaches. Metformin was selected as the reference antidiabetic agent, while PA—an enteric-soluble short-chain fatty acid (SCFA) known to improve fasting glucose, body weight, and insulin sensitivity [53]—was chosen to test a gut–brain-axis-based strategy for addressing T2DM-associated neuropathy. Because the direct effects of PA on VMH neurons in diabetes have not been fully defined, we employed an integrated approach combining ultrastructural and molecular analyses of apoptosis–autophagy dynamics.

HFD-fed rodents provided an appropriate model to assess how metformin and PA affect metabolic and neuronal responses. As expected, rats with HFD-induced T2DM showed marked VMH alterations: dilation of rough ER tubules and cisternae, accumulation of fragmented mitochondria with disrupted cristae and swollen matrices, and the presence of pyknotic nuclei. Together, these structural abnormalities resulted in more apoptotic neurons and loss of dendritic processes. These cellular findings corresponded with a molecular imbalance favoring apoptosis: notably, a strong increase in Bax—which translocates to mitochondria, oligomerizes, and promotes cytochrome c release—and in caspase-3, consistent with electron-microscopy observations. Meanwhile, levels of the autophagy marker LC3 and anti-apoptotic Bcl-xl were slightly reduced, indicating suppressed autophagic activity. Thus, T2DM promoted apoptotic activation and autophagy inhibition in the VMH, potentially contributing to defective glucose homeostasis and neuropathic outcomes. These findings align with previous evidence that high-fat diets can induce neuronal apoptosis [54]. Moreover, hypothalamic and brain-wide cell death may promote metabolic inflammation, which in turn contributes to central leptin and insulin resistance, precipitating overeating, glucose dysregulation, and hypertension.

Our results partly supported the initial hypothesis that pharmacological intervention would attenuate diabetes-related hypothalamic injury by reducing mitochondrial swelling and lowering the number of apoptotic neurons while enhancing glial responsiveness. This corresponds with prior research indicating that metformin exerts neuroprotective effects in primary cortical neurons [55]. To our knowledge, this is the first investigation into how metformin influences the apoptosis–autophagy shift specifically in the VMH under diabetic conditions. Metformin treatment produced swelling of myelinated fibers, increased autophagosomes and lysosomes, and reduced the size of ER cisternae relative to untreated diabetic animals. These signs of activated autophagy

correlated with increased levels of Bcl-xl, LC3, and Beclin-1, and decreased levels of Bax and caspase-3. However, metformin also led to undesirable changes, including the accumulation of lipofuscin granules—an aging-related marker associated with impaired stress responses, inflammasome activation, enhanced oxidative stress, and neuronal deterioration—and the development of reactive astrogliosis. Additionally, research in Caenorhabditis elegans and human cells has shown that metformin can disrupt conserved metabolic pathways in aging and contribute to mitochondrial dysfunction [56]. Thus, although metformin improved hyperglycemia, it did not fully prevent diabetes-induced VMH damage. This motivated further testing of PA as an adjunct neuroprotective therapy to mitigate metformin-related drawbacks and counteract neurodegenerative processes.

PA produced VMH changes similar to those seen with metformin but with greater magnitude. Numerous autophagosomes were noted, and the number of apoptotic cells was reduced compared with the T2DM group. These structural findings matched substantial increases in LC3 and Beclin-1, suggesting robust autophagy activation, and an increase in Bcl-xl to near-control levels. Despite fewer apoptotic neurons, PA unexpectedly increased both monomeric and total Bax, as well as caspase-3, suggesting a tendency toward apoptotic signaling that did not translate into morphological evidence of apoptosis. Because Bax can interact with Beclin-1 to inhibit autophagy [47], it may represent another critical point of crosstalk. Importantly, although Bax can oligomerize to induce mitochondrial apoptosis, we observed elevated Bax monomer rather than dimer, which may explain the lack of apoptotic features under electron microscopy. Another positive outcome was that astrocytes showed no signs of swelling, in contrast to the metformin group. Overall, these data reinforced our earlier hypothesis [13] that PA confers neuroprotection by stimulating autophagy and enhancing anti-apoptotic mechanisms, thereby preventing the accumulation of misfolded proteins.

Unexpected findings emerged from the combined metformin + PA treatment. Although we anticipated greater effectiveness than either drug alone [13], the combined therapy produced an increase in microglial density and a notable reduction in the proportion of healthy “light” neurons relative to controls. Nevertheless, the combination therapy slightly lowered the number of pre-apoptotic and apoptotic neurons compared with the metformin-only and PA-only groups. These structural observations were consistent with reduced caspase-3 and both monomeric and dimeric Bax, indicating diminished apoptosis. The highest Bcl-xl levels observed across all groups suggest that apoptosis was strongly inhibited via Bcl-xl activation. Because Bcl-xl also suppresses autophagy through interactions with Beclin-1 and Bax, sustained elevations of LC3 and Beclin-1 indicate that autophagy remained activated despite this inhibition. Altogether, the combination treatment produced what appears to be the most favorable balance of pro- and anti-apoptotic and autophagy markers in the VMH of diabetic rats.

Although we aimed to characterize VMH apoptosis and autophagy as thoroughly as possible, several limitations must be acknowledged. Due to the very small size of VMH samples, immunohistochemistry could not be performed for all proteins; we therefore restricted visualization to the Bax/Bcl-xl axis. Furthermore, although caspase-3 is commonly used as an apoptotic marker, it also plays non-apoptotic roles in certain brain cell types, including differentiation, cell-cycle regulation, and migration [57]. In the CNS, caspase-3 is also involved in cytoskeletal remodeling in neurons and astrocytes [58] as well as astrocyte-subpopulation differentiation. Future studies should distinguish apoptotic from non-apoptotic caspase-3 signaling under diabetic conditions and after metformin and PA treatment. Additional research is also needed to clarify the mechanisms through which PA influences the VMH.

In conclusion, our findings confirm that T2DM induces apoptosis and structural deterioration in the VMH. Diabetes-related dysregulation of pro- and anti-apoptotic proteins appears more pronounced at the protein level than at the transcriptional level, underscoring the importance of transcriptional stability. PA shifted the balance from apoptosis toward autophagy, supporting its neuroprotective potential during T2DM progression. Taken together, these results suggest that combined PA and metformin therapy may offer benefits in modulating hypothalamic cell-death pathways during the development of T2DM.

Conclusion

Our findings demonstrate that T2DM triggers intense apoptosis and mitoptosis in VMH neurons, which likely contributes to hypothalamic neuronal dysfunction. Although all treatments produced only modest improvements in VMH ultrastructure, they exerted clear effects on cell-fate regulation.

Metformin alone reduced neuronal apoptosis but simultaneously promoted cellular aging, evidenced by pronounced lipofuscin accumulation and residual debris in VMH neurons. In contrast, propionic acid (PA) more

effectively restored VMH cytoarchitecture and shifted the predominant cell-death pathway from apoptosis toward protective autophagy—an adaptive response that counteracted diabetes-induced damage. The combination of PA and metformin proved most beneficial, simultaneously suppressing apoptosis and stimulating autophagy.
Thus, both PA alone and, especially, its combination with metformin effectively protect VMH neurons against diabetes-related cell death by inhibiting apoptosis and promoting autophagy. These results position propionic acid as a promising neuroprotective adjunct to metformin for ameliorating diabetic encephalopathy and hypothalamic dysfunction through targeted modulation of the apoptosis–autophagy balance.

Acknowledgments: We would like to thank Prof., Dr. Nina Babel (Center for Translational Medicine and Immune Diagnostics Laboratory, Medical Department I, Marien Hospital Herne, University Hospital of the Ruhr University Bochum, Herne, Germany) for providing the sodium salt of propionic acid (PROPICUM®, Flexopharm Brain GmbH & Co, Germany). In addition, special thanks to all participants for their contribution.

Conflict of Interest: None

Financial Support: Nina Babel was supported by BMBF TriDiMeD [FKZ 01DK20008], NoChro [FKZ 13GW0338B]. Prof Larysa Natrus was supported by Research grant of the Ministry of Health of Ukraine [0122U001442].

Ethics Statement: None

References

1. U. Galicia-Garcia, A. Benito-Vicente, S. Jebari, et al., Pathophysiology of type 2 diabetes mellitus, Int. J. Mol. Sci. 21 (17) (2020) 6275.
2. E.L. Feldman, B.C. Callaghan, R. Pop-Busui, et al., Diabetic neuropathy, Nat. Rev. Dis. Prim. 5 (1) (2019) 42.
3. C.L. Boulange´, A.L. Neves, J. Chilloux, J.K. Nicholson, M.E. Dumas, Impact of the gut microbiota on inflammation, obesity, and metabolic disease, Genome Med. 8 (1) (2016) 42.
4. D. Zhang, S. Jiang, H. Meng, Role of the insulin-like growth factor type 1 receptor in the pathogenesis of diabetic encephalopathy, Internet J. Endocrinol. 2015 (2015), 626019.
5. D. Cai, T. Liu, Hypothalamic inflammation: a double-edged sword to nutritional diseases, Ann. N. Y. Acad. Sci. 1243 (2011) E1–E39.
6. D. Cai, Neuroinflammation and neurodegeneration in overnutrition-induced diseases, Trends Endocrinol. Metabol. 24 (1) (2013) 40–47.
7. M.H. Rahman, A. Bhusal, W.H. Lee, I.K. Lee, K. Suk, Hypothalamic inflammation and malfunctioning glia in the pathophysiology of obesity and diabetes: translational significance, Biochem. Pharmacol. 153 (2018) 123–133.
8. V. Poitout, R.P. Robertson, Glucolipotoxicity: fuel excess and beta-cell dysfunction, Endocr. Rev. 29 (3) (2008) 351–366.
9. V.K. Pandey, A. Mathur, P. Kakkar, Emerging role of Unfolded Protein Response (UPR) mediated proteotoxic apoptosis in diabetes, Life Sci. 216 (2019) 246–258.
10. C. He, D.J. Klionsky, Regulation mechanisms and signaling pathways of autophagy, Annu. Rev. Genet. 43 (2009) 67–93.
11. C. Liu, D.Y. Yan, C. Wang, Z. Ma, Y. Deng, W. Liu, B. Xu, Manganese activates autophagy to alleviate endoplasmic reticulum stress–induced apoptosis via PERK pathway, J. Cell Mol. Med. 24 (2020) 328–341.
12. W. Zheng, W. Xie, D. Yin, R. Luo, M. Liu, F. Guo, ATG5 and ATG7 induced autophagy interplays with UPR via PERK signaling, Cell Commun. Signal. 17 (2019) 42.
13. L.V. Natrus, YuS. Osadchuk, O.O. Lisakovska, D.O. Labudzinskyi, YuG. Klys, Chaikovsky YuB, Effect of propionic acid on diabetes-induced impairment of unfolded protein response signaling and astrocyte/microglia crosstalk in rat ventromedial nucleus of the hypothalamus, Neural Plast. 2022 (2022). Article ID 6404964.
14. Y. Chun, J. Kim, Autophagy: an essential degradation program for cellular homeostasis and life, Cells 7 (12)

(2018) 278.
15. K.R. Parzych, D.J. Klionsky, An overview of autophagy: morphology, mechanism, and regulation, Antioxidants Redox Signal. 20 (3) (2014) 460–473.
16. M. Li, P. Gao, J. Zhang, Crosstalk between autophagy and apoptosis: potential and emerging therapeutic targets for cardiac diseases, Int. J. Mol. Sci. 17 (3) (2016) 332.
17. D. Bhattacharya, M. Mukhopadhyay, M. Bhattacharyya, P. Karmakar, Is autophagy associated with diabetes mellitus and its complications? A review, EXCLI J 17 (2018) 709–720.
18. F. Navone, P. Genevini, N. Borgese, Autophagy and neurodegeneration: insights from a cultured cell model of ALS, Cells 4 (3) (2015) 354–386.
19. J. Lim, Z. Yue, Neuronal aggregates: formation, clearance, and spreading, Dev. Cell 32 (4) (2015) 491–501.
20. Y. Cai, J. Arikkath, L. Yang, M.L. Guo, P. Periyasamy, S. Buch, Interplay of endoplasmic reticulum stress and autophagy in neurodegenerative disorders, Autophagy 12 (2) (2016) 225–244.
21. P. Sweeney, H. Park, M. Baumann, et al., Protein misfolding in neurodegenerative diseases: implications and strategies, Transl. Neurodegener. 6 (2017) 6.
22. M.P. Zhang, W.H. Wu, Q. Zhang, X.J. Li, Q.D. Hu, S.J. Yang, L. Xue, The study on the beclin1 expression and change in diabetic rats, Sichuan Da Xue Xue Bao Yi Xue Ban 42 (4) (2011), 508-510, 522.
23. Z.F. Guan, X.L. Zhou, X.M. Zhang, et al., Beclin-1- mediated autophagy may be involved in the elderly cognitive and affective disorders in streptozotocin-induced diabetic mice, Transl. Neurodegener. 5 (2016) 22.
24. G. Runwal, E. Stamatakou, F.H. Siddiqi, C. Puri, Y. Zhu, D.C. Rubinsztein, LC3- positive structures are prominent in autophagy-deficient cells, Sci. Rep. 9 (1) (2019), 10147.
25. N. Fujikake, M. Shin, S. Shimizu, Association between autophagy and neurodegenerative diseases, Front. Neurosci. 12 (2018) 255.
26. G.Y. Wang, Y.G. Bi, X.D. Liu, et al., Autophagy was involved in the protective effect of metformin on hyperglycemia-induced cardiomyocyte apoptosis and Connexin43 downregulation in H9c2 cells, Int. J. Med. Sci. 14 (7) (2017) 698–704.
27. B. Levine, S. Sinha, G. Kroemer, Bcl-2 family members: dual regulators of apoptosis and autophagy, Autophagy 4 (5) (2008) 600–606.
28. K. Mahmood, M. Naeem, N.A. Rahimnajjad, Metformin: the hidden chronicles of a magic drug, Eur. J. Intern. Med. 24 (1) (2013) 20–26.
29. C. Wang, C. Liu, K. Gao, H. Zhao, Z. Zhou, Z. Shen, Y. Guo, Z. Li, T. Yao, X. Mei, Metformin preconditioning provide neuroprotection through enhancement of autophagy and suppression of inflammation and apoptosis after spinal cord injury, Biochem. Biophys. Res. Commun. 477 (4) (2016) 534–540.
30. C.C. Lu, J.H. Chiang, F.J. Tsai, Y.M. Hsu, Y.N. Juan, J.S. Yang, H.Y. Chiu, Metformin triggers the intrinsic apoptotic response in human AGS gastric adenocarcinoma cells by activating AMPK and suppressing mTOR/AKT signaling, Int. J. Oncol. 54 (4) (2019) 1271–1281.
31. M.A.G. Hern´andez, E.E. Canfora, J.W.E. Jocken, E.E. Blaak, The short-chain fatty acid acetate in body weight control and insulin sensitivity, Nutrients 11 (8) (2019) 1943.
32. M.M. Sharmin, M. Mizusawa, S. Hayashi, W. Arai, S. Sakata, S. Yonekura, Effects of fatty acids on inducing endoplasmic reticulum stress in bovine mammary epithelial cells, J. Dairy Sci. 103 (9) (2020) 8643–8654.
33. A.K. El-Ansary, A. Ben Bacha, M. Kotb, Etiology of autistic features: the persisting neurotoxic effects of propionic acid, J. Neuroinflammation 9 (2012) 74.
34. L. Natrus, Osadchuk Yu, D. Labudzinskyi, Chaikovsky Yu, A. Smirnov, The pathogenetic rationale of the ways of experimental type 2 diabetes mellitus modeling, Med. Sci. Ukr. 15 (3-4) (2019) 10–18.
35. F. Zou, X.Q. Mao, N. Wang, J. Liu, J.P. Ou-Yang, Astragalus polysaccharides alleviates glucose toxicity and restores glucose homeostasis in diabetic states via activation of AMPK, Acta Pharmacol. Sin. 30 (12) (2009) 1607–1615.
36. T. Zhang, B.S. Pan, B. Zhao, L.M. Zhang, Y.L. Huang, F.Y. Sun, Exacerbation of poststroke dementia by type 2 diabetes is associated with synergistic increases of beta-secretase activation and beta-amyloid generation in rat brains, Neuroscience 161 (4) (2009) 1045–1056.
37. S.H. Hu, T. Jiang, S.S. Yang, Y. Yang, Pioglitazone ameliorates intracerebral insulin resistance and tau-protein hyperphosphorylation in rats with type 2 diabetes, Exp. Clin. Endocrinol. Diabetes 121 (4) (2013)

220–224.
38. S. Skovsø, Modeling type 2 diabetes in rats using high fat diet and streptozotocin, J. Diabetes Investig. 5 (4) (2014) 349–358.
39. A. Haghikia, S. Jo€rg, A. Duscha, J. Berg, A. Manzel, A. Waschbisch, A. Hammer, D.H. Lee, C. May, N. Wilck, A. Balogh, A.I. Ostermann, N.H. Schebb, D.A. Akkad, D.A. Grohme, M. Kleinewietfeld, S. Kempa, J. Tho€ne, S. Demir, D.N. Müller, R. Gold, R.A. Linker, Dietary fatty acids directly impact central nervous system autoimmunity via the small intestine, Immunity 43 (4) (2015) 817–829.
40. M.A. Hayat, Principles and Techniques of Electron Microscopy: Biological Applications, fourth ed., Cambridge University Press, New York, 2000.
41. I. Tanida, T. Ueno, E. Kominami, LC3 conjugation system in mammalian autophagy, Int. J. Biochem. Cell Biol. 36 (12) (2004) 2503–2518.
42. R. Kang, H.J. Zeh, M.T. Lotze, D. Tang, The Beclin 1 network regulates autophagy and apoptosis, Cell Death Differ. 18 (4) (2011) 571–580.
43. M.B. Menon, S. Dhamija, Beclin 1 phosphorylation - at the center of autophagy regulation, Front. Cell Dev. Biol. 6 (2018) 137.
44. Y. Subburaj, K. Cosentino, M. Axmann, et al., Bax monomers form dimer units in the membrane that further self-assemble into multiple oligomeric species, Nat. Commun. 6 (2015) 8042.
45. W.C. Earnshaw, L.M. Martins, S.H. Kaufmann, Mammalian caspases: structure, activation, substrates, and functions during apoptosis, Annu. Rev. Biochem. 68 (1999) 383–424.
46. S. Narkilahti, T.J. Pirttila€, K. Lukasiuk, J. Tuunanen, A. Pitka€nen, Expression and activation of caspase 3 following status epilepticus in the rat, Eur. J. Neurosci. 18 (6) (2003) 1486–1496.
47. M.C. Maiuri, G. Le Toumelin, A. Criollo, J.C. Rain, F. Gautier, P. Juin, E. Tasdemir,
48. G. Pierron, K. Troulinaki, N. Tavernarakis, J.A. Hickman, O. Geneste, G. Kroemer, Functional and physical interaction between Bcl-X(L) and a BH3-like domain in Beclin-1, EMBO J. 26 (10) (2007) 2527–2539.
49. F. Zhou, Y. Yang, D. Xing, Bcl-2 and Bcl-xL play important roles in the crosstalk between autophagy and apoptosis, FEBS J. 278 (3) (2011) 403–413.
50. L.A. Booth, S. Tavallai, H.A. Hamed, N. Cruickshanks, P. Dent, The role of cell signalling in the crosstalk between autophagy and apoptosis, Cell. Signal. 26 (3) (2014) 549–555.
51. E. Wong, A.M. Cuervo, Autophagy gone awry in neurodegenerative diseases, Nat. Neurosci. 13 (7) (2010) 805–811.
52. E. Heimann, M. Nyman, E. Degerman, Propionic acid and butyric acid inhibit lipolysis and de novo lipogenesis and increase insulin-stimulated glucose uptake in primary rat adipocytes, Adipocyte 4 (2) (2014) 81–88.
53. J.C. Moraes, A. Coope, J. Morari, D.E. Cintra, E.A. Roman, J.R. Pauli, T. Romanatto, J.B. Carvalheira, A.L. Oliveira, M.J. Saad, L.A. Velloso, High-fat diet induces apoptosis of hypothalamic neurons, PLoS One 4 (4) (2009), e5045.
54. M.Y. El-Mir, D. Detaille, G. R-Villanueva, M. Delgado-Esteban, B. Guigas, S. Attia, E. Fontaine, A. Almeida, X. Leverve, Neuroprotective role of antidiabetic drug metformin against apoptotic cell death in primary cortical neurons, J. Mol. Neurosci. 34 (1) (2008) 77–87.
55. L. Espada, A. Dakhovnik, P. Chaudhari, A. Martirosyan, L. Miek, T. Poliezhaieva, Y. Schaub, A. Nair, N. Do€ring, N. Rahnis, O. Werz, A. Koeberle, J. Kirkpatrick, A. Ori, M.A. Ermolaeva, Loss of metabolic plasticity underlies metformin toxicity in aged Caenorhabditis elegans, Nat. Metab 2 (11) (2020 Nov) 1316–1331.
56. X. Zhao, D. Wang, Z. Zhao, Y. Xiao, S. Sengupta, Y. Xiao, R. Zhang, K. Lauber, S. Wesselborg, L. Feng, T.M. Rose, Y. Shen, J. Zhang, G. Prestwich, Y. Xu, Caspase-3- dependent activation of calcium-independent phospholipase A2 enhances cell migration in non-apoptotic ovarian cancer cells, J. Biol. Chem. 281 (39) (2006) 29357–29368.
57. L. Acarin, S. Villapol, M. Faiz, T.T. Rohn, B. Castellano, B. Gonz´alez, Caspase-3 activation in astrocytes following postnatal excitotoxic damage correlates with cytoskeletal remodeling but not with cell death or proliferation, Glia 55 (9) (2007) 954–965.
58. S. Oomman, H. Strahlendorf, J. Dertien, J. Strahlendorf, Bergmann glia utilize active caspase-3 for differentiation, Brain Res. 1078 (1) (2006) 19–34.